Supporting Information

Silver-Overgrowth-Induced Changes in Intrinsic Optical Properties of Gold Nanorods: From Noninvasive Monitoring of Growth Kinetics to Tailoring Internal Mirror Charges

Moritz Tebbe,[a] Christian Kuttner,[a] Martin Mayer,[a] Max Maennel,[a] Nicolas Pazos-Perez,[a,b] Tobias A.F. König,[a] and Andreas Fery[a]**

[a] Physical Chemistry II, University of Bayreuth, Universitätsstraße 30, 95440 Bayreuth, Germany.

[b] Departamento de Quimica Fisica e Inorganica, Universitat Rovira i Virgili and Centro de Tecnologia Quimica de Cataluña, Carrer de Marcel•lí Domingo s/n, 43007 Tarragona, Spain.

* To whom correspondence should be addressed

E-mail (T.K.): tobias.koenig@uni-bayreuth.de; E-mail (A.F.): andreas.fery@uni-bayreuth.de.

The following section provides further information about the experimental results and electromagnetic simulations of nanoparticle synthesis and silver overgrowth discussed in the main text. Additionally, information on performed kinetic experiments and corresponding data evaluation is provided.

Gold Nanorod Characterization

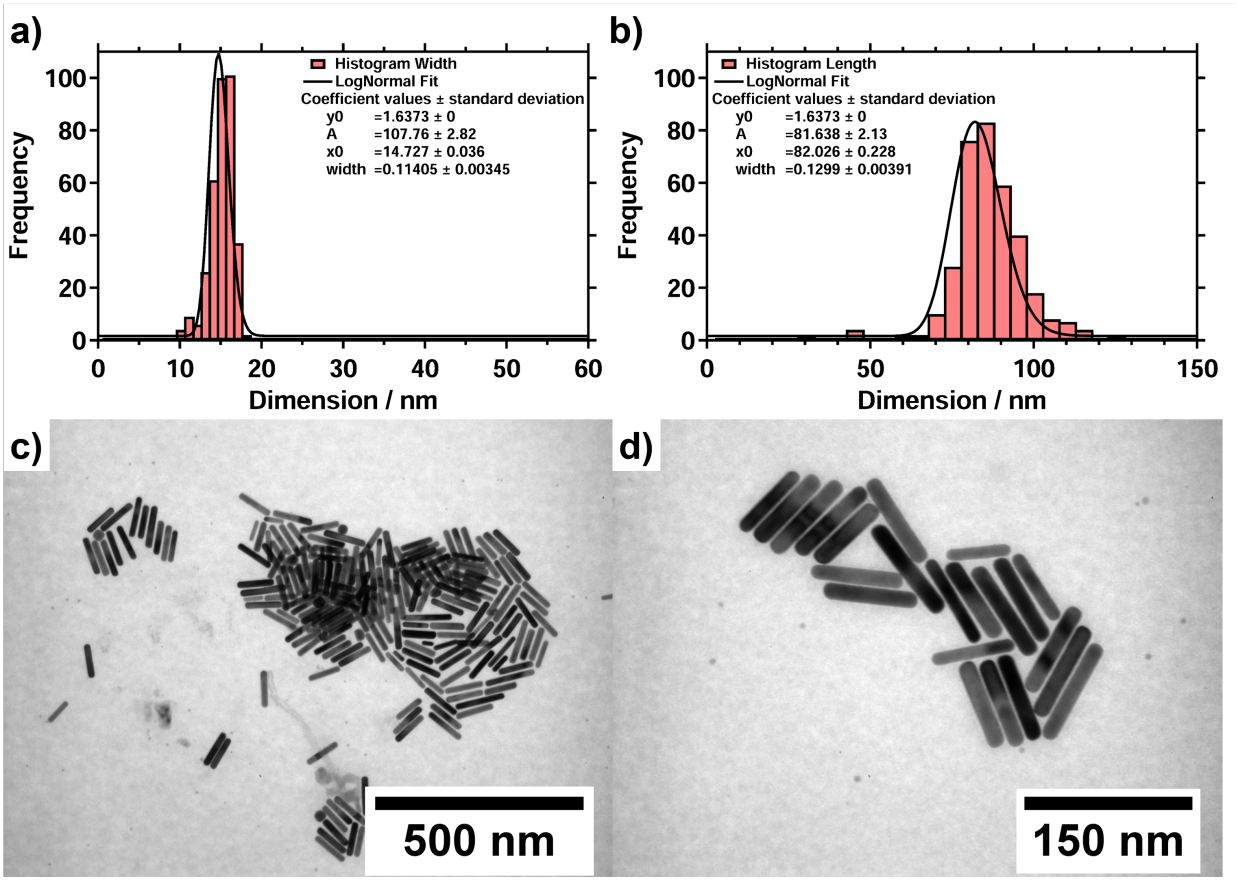

Figure S1. CTAB-based gold nanorod synthesis with hydroquinone.[1] (a/b) Histograms of the width and length distribution of as prepared gold nanoparticles (n=150). (c/d) Low- and high-magnification TEM images of as-prepared gold nanorods.

FDTD Modeling of Gold Nanorods

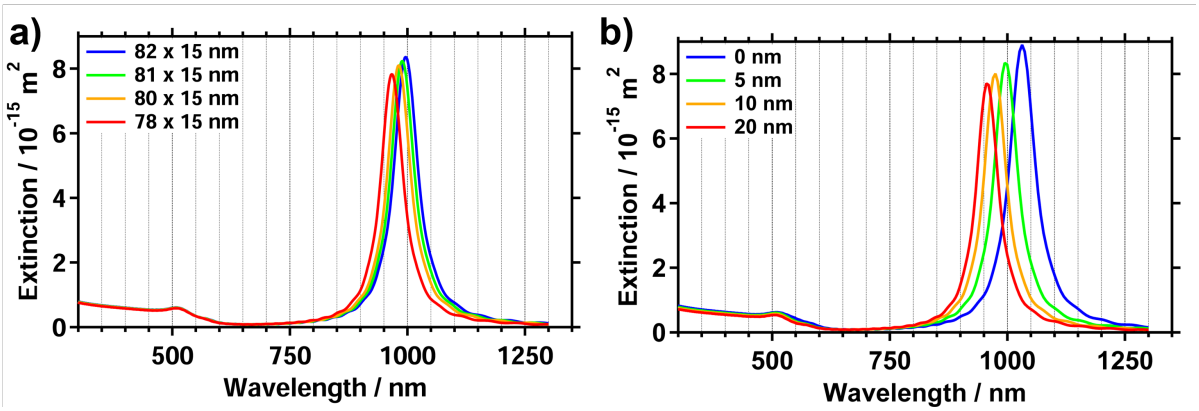

Figure S2. Finite-difference time-domain (FDTD) modeling for gold nanorods performed on the basis of dielectric data taken from Johnson and Christy (JC).[2] (a) Modeled extinction spectra of gold nanorods with 5 nm tip rounding with fixed width and varied length (75-82 nm). (b) Modeled extinction spectra of gold nanorods for fixed length (82 nm) and width (15 nm) with varied tip rounding values (0-15 nm).

Silver Overgrowth Characterization

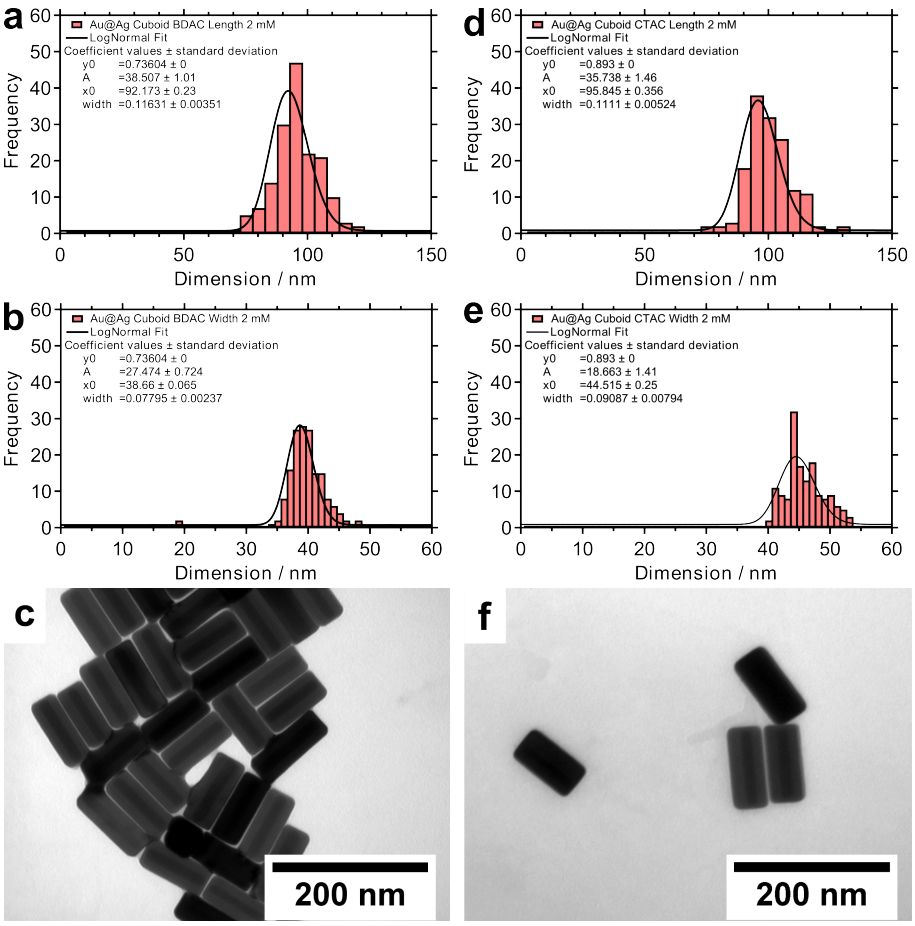

Figure S3. Silver overgrowth of gold nanorods in 10 mM CTAC or BDAC at 60 °C and with a final Ag to Au ratio of 8 ([Ag] = 2 mM). (a/b) Distribution of the width and length of silver overgrowth performed with BDAC plotted as histograms. (c) TEM micrograph of as prepared cuboids in BDAC. (d/e) Distribution of the width and length of silver overgrowth performed with CTAC plotted as histograms. (f) TEM micrograph of as-prepared cuboids in CTAC.

FDTD Modeling of Au@Ag Cuboids

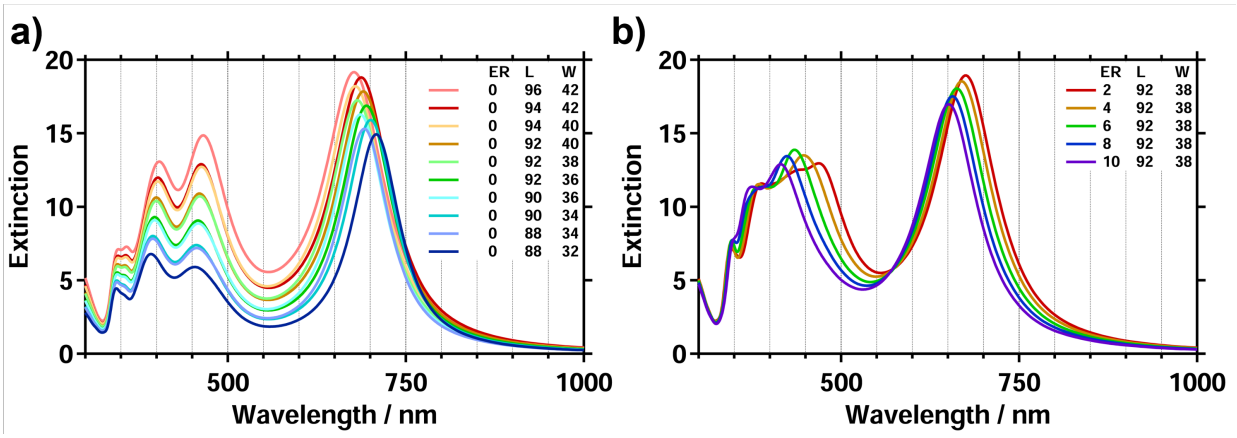

Figure S4. FDTD modeling of Au@Ag cuboids, focused on small variations in dimension and edge rounding. (a) Modeled extinction spectra of Au@Ag cuboids with 0% edge rounding and varied width and length (88-96 nm and 32-42 nm). (b) Modeled extinction spectra of Au@Ag cuboids with fixed width and length (92 nm and 38 nm) and varied edge rounding values (2-10%).

Evaluation of Static Overgrowth Experiments

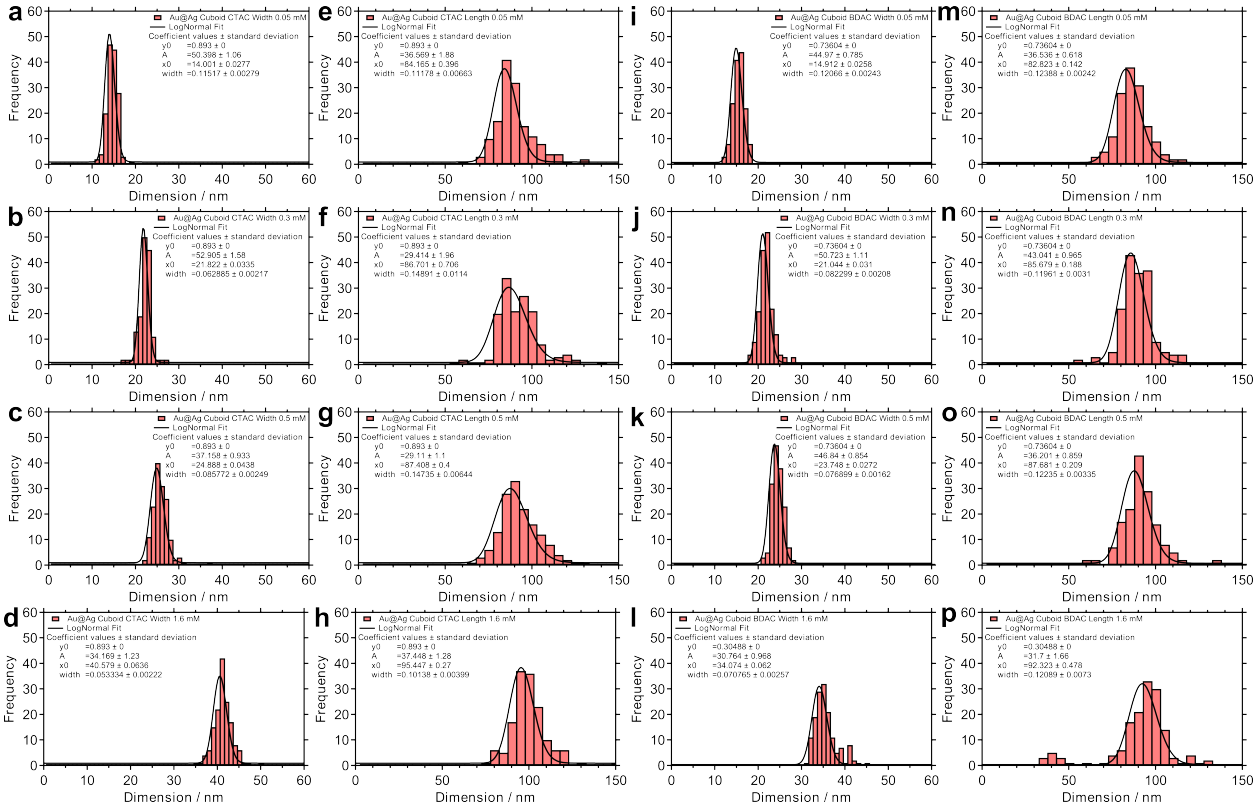

Figure S5. Silver overgrowth of gold nanorods with 10 mM surfactant, at 60 °C for varied silver amounts. Distribution of the (a-d) width and (e-f) length of Au@Ag cuboids prepared with CTAC plotted as histograms (n = 150). Distribution of the (i-l) width and (m-p) length of Au@Ag cuboids prepared with BDAC plotted as histograms (n = 150). (Ag to Au ratio: (a/e/i/m) 0.2; (b/f/j/n) 1.2; (c/g/k/o) 2; (d/h/l/p) 6.4).

Au@Ag Cuboid Growth Kinetics 3D Plots

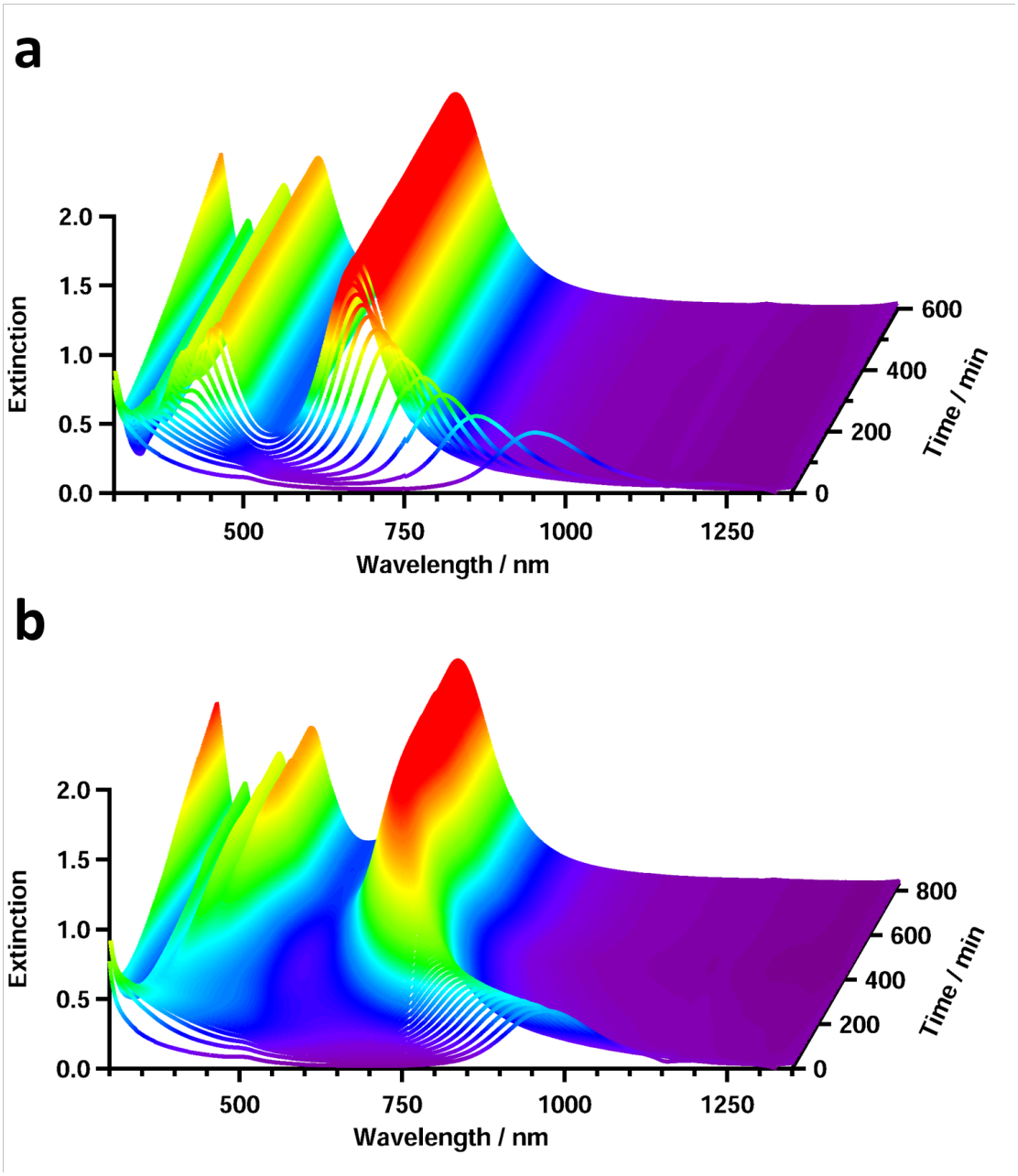

Figure S6. Au@Ag cuboid growth in dynamic experiments: 3D representation of heat-maps (Figure 4a/b) of time-dependent UV/vis/NIR extinction spectra of synthesis performed with (a) CTAC and (b) BDAC at Ag to Au ratio of 8. (a)

Au@Ag Cuboid Growth Kinetics TEM Evaluation

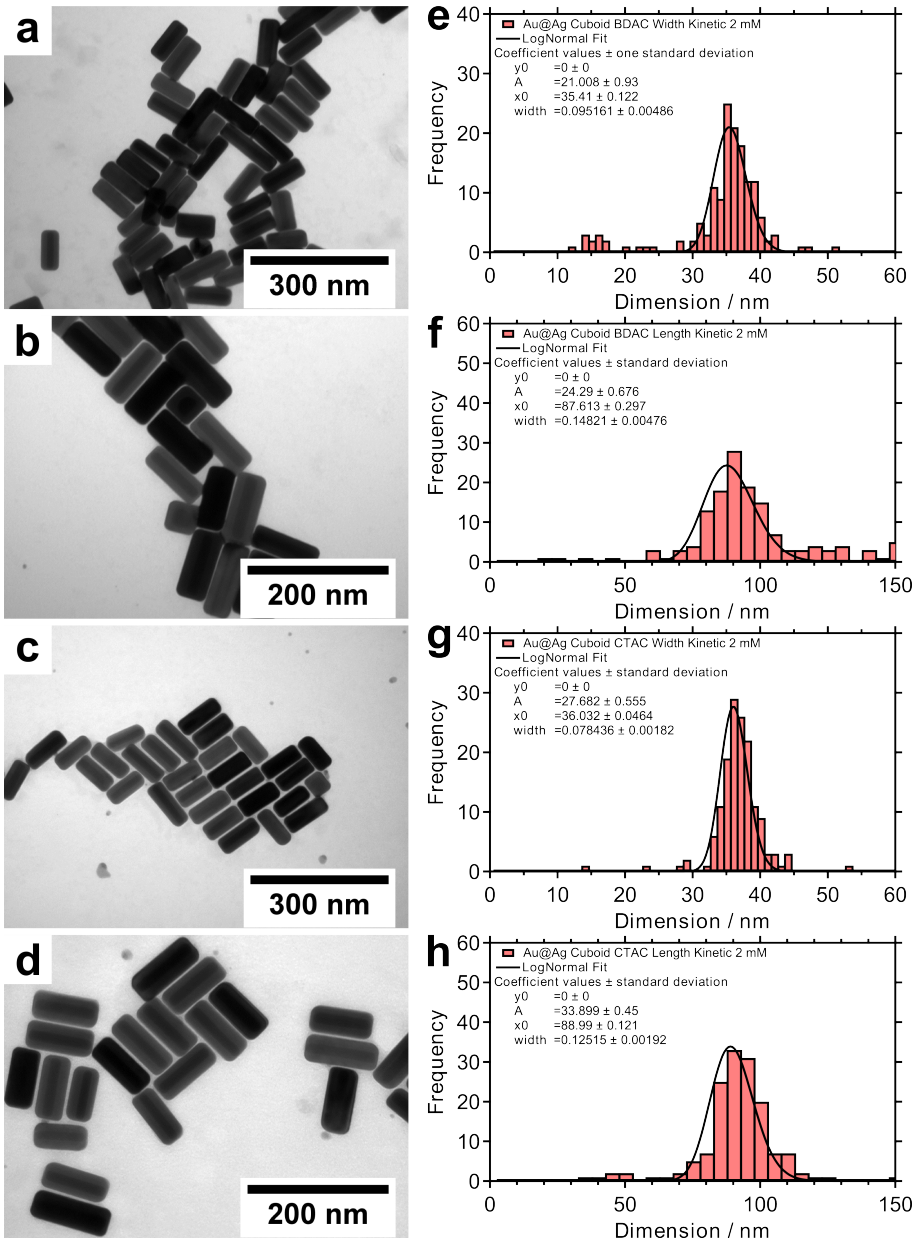

Figure S7. TEM micrographs and histograms of as-prepared Au@Ag cuboid kinetic experiments. TEM images obtained for (a/b) BDAC and (c/d) CTAC. Histograms of the (e) width and (f) length of BDAC and for the (g) width and (h) length of CTAC obtained by measuring 150 nanoparticles.

Modeling of Au@Ag Cuboid Growth Kinetics

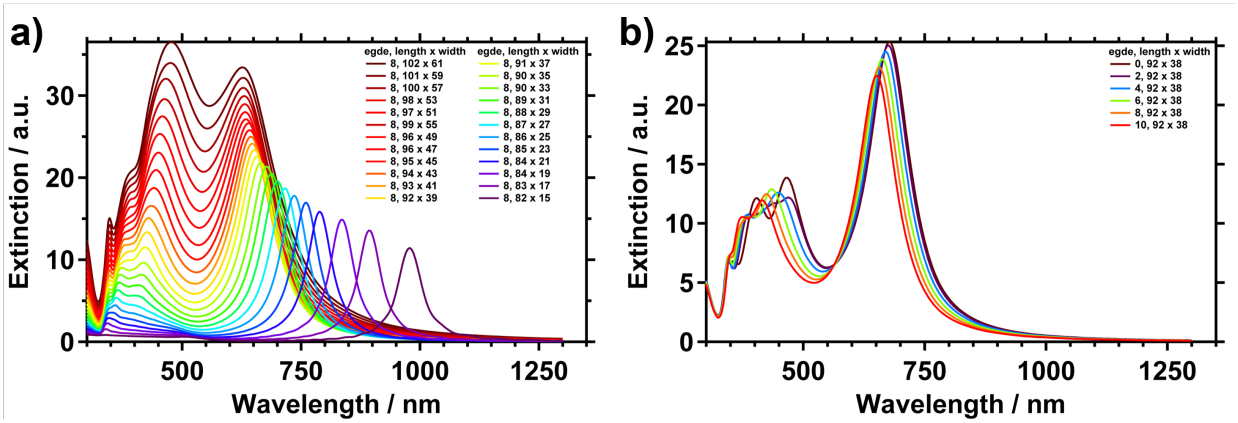

Figure S8. (a) Extended plot of the FDTD modeling of Au@Ag cuboids performed including linear overgrowth up to 101 nm in length and 55 nm in width. (b) Modeled extinction spectra of cuboids with a fixed width and length (92 nm and 38 nm) and varied edge rounding values (0-10%).

Table S1. FDTD simulation parameters as used for the kinetic plot in **Figure 4**.

Total length / nm	Total width / nm	Edge rounding / %
82	**15**	8
83	**17**	8
84	**19**	8
84	**21**	8
85	**23**	8
86	**25**	8
87	**27**	8
88	**29**	8
89	**31**	8
90	**33**	8
90	**35**	8
91	**37**	8
92	**38**	8
92	38	**6**
92	38	**4**
92	38	**2**
92	38	**0**

Evaluation of Au@Ag Cuboid Growth Kinetics

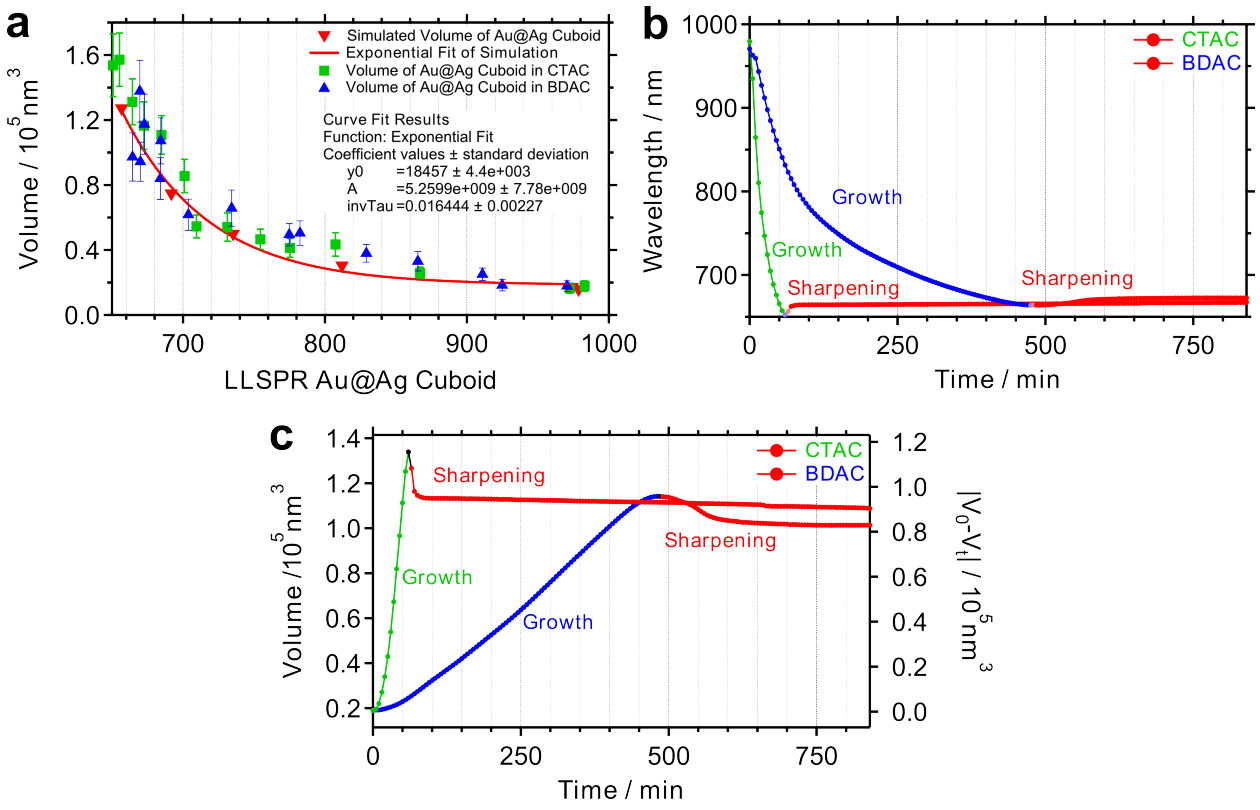

Figure S9. Systematic evaluation of kinetic experiments based on results for static experiments. Experimentally determined (CTAC: green squares; BDAC: blue triangles) and modeled (red) Au@Ag cuboid volumes plotted versus their longitudinal resonance mode. (a) Modeled values were fitted with an exponential fit. (b) The longitudinal resonance mode of kinetic experiments performed with CTAC (green) and BDAC (blue) plotted versus reaction time. (c) Calculated volumes of kinetic experiments plotted versus time. Calculations were performed on the basis of the experimentally determined longitudinal resonance mode shift of the kinetic experiments and exponential fit of the modeled cuboid volumes. Please note that volumes determined on basis of spectral data after the maximum value of the longitudinal resonance mode are not representing real changes in volume but are caused by sharpening of Au@Ag cuboid edges.

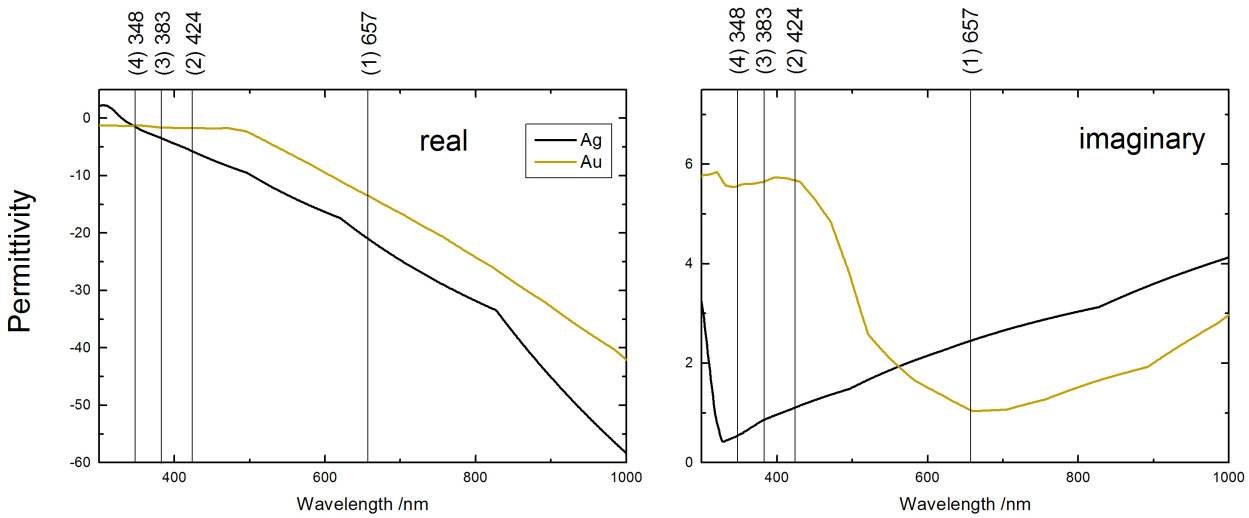

Figure S10: Complex permittivity of silver (CRC) and gold (JC), which were used in the simulations. Labels (1-4) mark the wavelengths of the transversal and longitudinal modes.

Text S1: Mirror Charges at Au@Ag Gold-Core/Silver-Shell Nanoparticles

We established a mirror charge model for Au@Ag gold-core/silver-shell cuboids based on the calculation of surface charge plots (normalized surface charge density, $\rho_n = \mathrm{Re}[\nabla \vec{E}]$). **Figures S11-13** show the comparison of the plasmonic modes (gold nanorod, Au@Ag cuboid, and silver cuboid) with the help of the electric field intensity. As typically for a plasmonic resonance the field intensity is exponentially decaying into the dielectric environment. A significant lower intensity part decays into the metal core (receiver) and shows a resonance coupling with the shell (antenna). The Au@Ag cuboid shows the expected alteration of the plasmonic resonance in comparison to a silver cuboid, due to the refractive index change from silver to gold. In other words, the electric field of the Au@Ag cuboid mode (2) (dominant field at the edged/corner) is slightly modified due to the gold core (**Figure S11**). The electric field of the Au@Ag cuboid mode (3) (dominant field at the faces) is clearly modified due to the gold core (**Figure S12**). Mode (4), which shows a dominant field at the faces is also clearly modified due to the gold core and form a charge free area at the center (**Figure S13**).

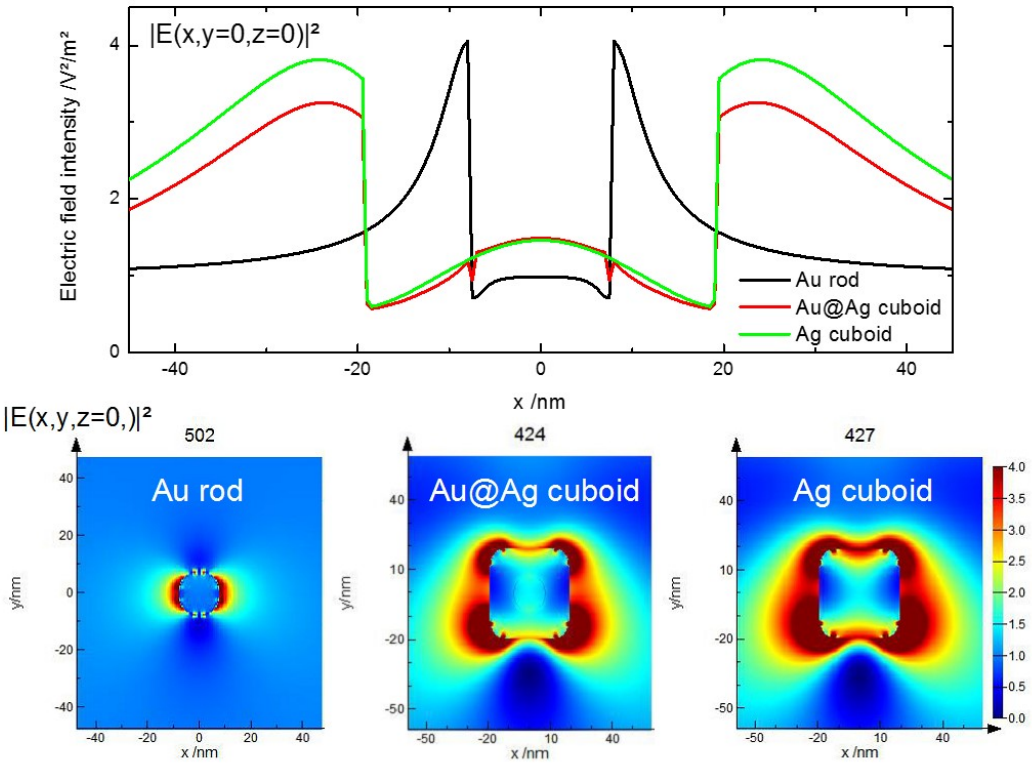

Figure S11: Electric field intensity cross-section and plane-plot of the gold nanorod (R_0^T), Au@Ag cuboid (2), and silver cuboid (C_0^T) plasmonic mode at their specific resonance wavelengths. Plane-plots are imaged with identical scale bars.

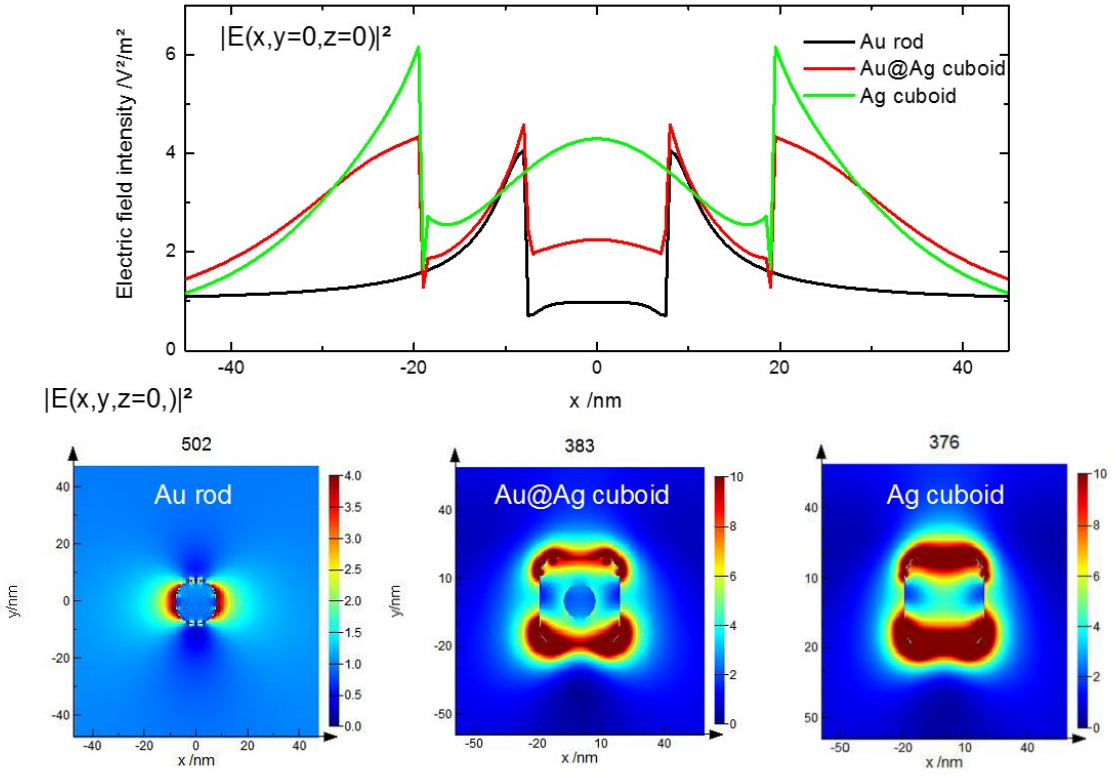

Figure S12: Electric field intensity cross-section and plane-plot of the gold nanorod (R_0^T), Au@Ag cuboid (3), and silver cuboid (C_1^T) plasmonic mode at their specific resonance wavelengths. Plane-plots are imaged with identical scale bars.

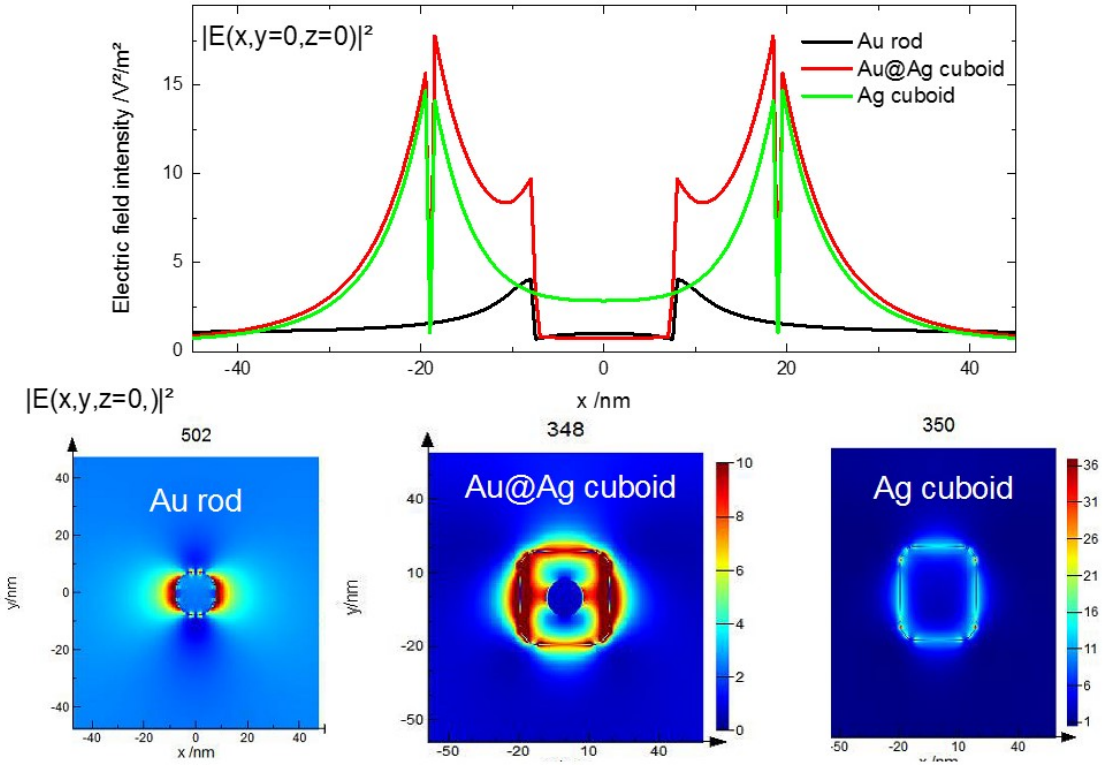

Figure S13: Electric field intensity cross-section and plane-plot of the gold nanorod (R_0^T), Au@Ag cuboid (4), and silver cuboid (C_2^T) plasmonic mode at their specific resonance wavelengths. Plane-plots are imaged with identical scale bars.

Table S2. Silver overgrowth synthesis parameters: Concentrations as used for static silver overgrowth experiments for both surfactants, BDAC and CTAC (10 mM) and at 60 °C. Parameters of synthesis #14 were also used for kinetic experiments.

Experiment	Au / mM	$AgNO_3$ / mM	AA / mM	Ag/Au ratio
1	0.25	0.05	0.2	**0.2**
2	0.25	0.1	0.4	**0.4**
3	0.25	0.2	0.8	**0.8**
4	0.25	0.3	1.2	**1.2**
5	0.25	0.4	1.6	**1.6**
6	0.25	0.5	2.0	**2.0**
7	0.25	0.6	2.4	**2.4**
8	0.25	0.8	3.2	**3.2**
9	0.25	1.0	4.0	**4.0**
10	0.25	1.2	5.0	**5.0**
11	0.25	1.4	5.6	**5.6**
12	0.25	1.6	6.4	**6.4**
13	0.25	1.8	7.2	**7.2**
14	**0.25**	**2.0**	**8.0**	**8.0**

References

1. Vigderman, L.; Zubarev, E. R. High-Yield Synthesis of Gold Nanorods with Longitudinal SPR Peak Greater than 1200 nm Using Hydroquinone as a Reducing Agent. *Chem. Mater.* **2013,** *25*, 1450-1457.
2. Johnson, P. B.; Christy, R. W. Optical Constants of the Noble Metals. *Phys. Rev. B* **1972,** *6*, 4370-4379.